Ferrisepiolite: a new mineral from Saishitang copper skarn deposit in Xinghai County, Qinghai Province, China

Gu Xiangping[1,2,*], Xie Xiande[1], Wu Xiangbin[2], Zhu Guchang[3], Lai Jianqing[2], Hoshino Kenich[4]
and Huang Jiwu[2]

[1] Guangzhou Institute of Geochemistry, Key Laboratory of Mineralogy and Metallogeny, Chinese Academy of Sciences, Wushan, Guangzhou City, Guangdong 510640, China
[2] School of Geosciences and Info-Physics, Central South University, Changsha, Hunan 410083, China
*Corresponding author, e-mail: guxp2004@163.com
[3] Beijing Technology Center of Exploration for Nonferrous Metals, Beiyuan, Beijing 10012, China
[4] Department of Earth & Planetary Sciences, Hiroshima University, Kagamiyama 1-3-1, Higashi Hiroshima City, Hiroshima Prefecture 739-8526, Japan

Abstract: Ferrisepiolite was discovered in the Saishitang copper skarn deposit in Xinghai County, Qinghai Province, China, as late-stage veinlets in copper-sulphide ores hosted in layered hedenbergite-andradite-actinolite skarn related to Indo-Sinian quartz diorite and Lower Permian metamorphosed clastic and carbonate rocks. Ferrisepiolite was formed in a highly oxidizing environment from low-temperature Fe-rich fluids and crystallized in cavities and fractures within the skarn-ore deposit. The mineral occurs in brown earthy and fibrous aggregates and shows brown to red-brown colour with strong pleochroism and 2nd order interference colours in a petrographic microscope. The measured refraction indices in white light for fibrous ferrisepiolite are: $\gamma' = 1.628(8)$, $\alpha' = 1.592$–1.620. The thermal analysis of ferrisepiolite reveals a lower dehydration temperature of structural hydroxyl than sepiolite and a small weight loss (0.1–0.9%) in the range 500–700 °C. The average chemical composition from wet chemistry, X-ray fluorescence spectrometry (XRF) and electron probe microanalysis (EPMA) is $(Fe^{3+}_{1.84},Fe^{2+}_{0.51},Mg_{1.56},Ca_{0.05},Mn_{0.02},Na_{0.02})_{\Sigma=4}$ $(Si_{5.79},Fe^{3+}_{0.21})_{\Sigma=6}O_{15}.(O_{1.60},OH_{0.40})_{\Sigma=2}\cdot6H_2O$ for fibrous ferrisepiolite and $(Fe^{3+}_{2.64},Fe^{2+}_{0.80},Mg_{0.35},Ca_{0.11},Mn_{0.05},Na_{0.05})_{\Sigma=4}$ $(Si_{5.18},Fe^{3+}_{0.82})_{\Sigma=6}O_{15}.(O_{1.77},OH_{0.23})_{\Sigma=2}\cdot6H_2O$ for earthy ferrisepiolite, which leads to the general formula: $(Fe^{3+},Fe^{2+},Mg)_4$ $(Si,Fe^{3+})_6O_{15}.(O,OH)_2\cdot6H_2O$. The powder X-ray diffraction (XRD) of ferrisepiolite is in agreement with that of sepiolite. The eight strongest lines of the pattern of fibrous ferrisepiolite are [d in Å (I)(hkl)]: 12.163(100)(110), 4.298(35)(131), 3.751(15)(260), 3.394(29)(400), 3.198(13)(331), 2.561(45)(191), 2.436(31)(212), 2.260(14)(391). Powder XRD and single-crystal electron-diffraction data show that ferrisepiolite is isostructural to sepiolite with orthorhombic unit-cell parameters (space group $Pncn$) $a = 13.619 (8)$, $b = 26.959 (26)$, $c = 5.241 (7)$ Å, $V = 1924.08$ Å^3, $Z = 4$, Dcal = 2.51 g/cm^3 for fibrous ferrisepiolite and $a = 13.638 (9)$ Å, $b = 27.011 (30)$ Å, $c = 5.233(8)$ Å, $V = 1927.58$ Å^3, $Z = 4$, Dcal = 2.69 g/cm^3 for earthy ferrisepiolite. Ferrisepiolite is the Fe(III)-dominant analogue of sepiolite with the substitution of Fe^{3+} and/or Fe^{2+} for Mg in the octahedral sites, compensated by substitution of Fe^{3+} for Si^{4+} in the tetrahedral sites and O^{2-} for OH^- in the sites of structural hydroxyl, accompanied by a contraction of the structure along the c-axis and an expansion along the a-axis.

Key-words: ferrisepiolite, new mineral, clay mineral, coupled substitution, copper skarn, Saishitang; China.

1. Introduction

Sepiolite is a magnesium phyllosilicate widely used in the pharmaceutical, fertilizer, construction and pesticide industries owing to its large surface area and microporosity. The substitution of Ni for Mg in the octahedral sites leads to the end-member falcondoite $(Ni,Mg)_4Si_6O_{15}(OH)_2\cdot6H_2O$ (Springer, 1976). However, high substitution of Fe for Mg, commonly observed in many other silicate minerals, is not often observed in sepiolite, and the iron analogue of sepiolite is not known. Fe-bearing sepiolites with various amounts of iron have been reported (Caillère, 1936; Bøggild, 1951; Brauner & Preisinger, 1956; Strunz, 1957; Preisinger, 1959; Semenov, 1969, Binzer & Karup-Møller, 1974; García-Romero & Suárez, 2010), but none has been approved as an independent mineral species by IMA-CNMNC because of lack of adequate data on chemical composition and crystal structure. Chukanova *et al.* (2002) reported an iron-rich analogue of sepiolite with the composition $Ca_{0.02}(Fe_{2.23}Mn_{1.06}Mg_{0.52}Zn_{0.17}Ti_{0.08})_{\Sigma4.06}(Si_{5.94}Al_{0.06})_{\Sigma6.00}O_{15}[(OH)_{1.74}O_{0.26}]_{\Sigma2.00}\cdot nH_2O$. which was probably an Fe(II)-dominant analogue of sepiolite as judged from the

chemical formula and was considered as a valid unnamed mineral (Smith & Nickel, 2007).

During a field survey on the Saishitang copper deposit in Xinghai County, Qinghai Province, China in August of 2006, an abundance of black pitchy or brown materials in the ores were assumed to be wood fossils. However, subsequent laboratory examination revealed that this material is an iron silicate mineral with the XRD pattern comparable to sepiolite. After further studies, a proposal for new mineral status with the name ferrisepiolite was submitted to and approved by the IMA-CNMNC (2010-061). The name, ferrisepiolite, indicates its structural relationship to sepiolite and the dominance of Fe (III). The name was originally used by Strunz (1957) to describe Fe-bearing sepiolite with Fe_2O_3 (14.57%) and FeO (1.06%), which was previously reported by Bøggild (1951) as a new mineral with the name ''gunnbjarnite''. Binzer & Karup-Møller (1974) presented data for a mineral with the name ''ferrisepiolite'' with Fe_2O_3 (9.98%) and FeO (1.18%). ''Xylotile'' and ''mountain wood'' were also used to describe sepiolite with considerable $Fe_2O_3 + FeO$ contents but less than 21.7% dominated by ferric iron (Caillère, 1936; Brauner & Preisinger, 1956). Occurrences of sepiolite with high contents of Fe and Mn in names ''Mn-ferrisepiolite'' and ''iron-rich analogue of sepiolite'', probably with dominant ferrous iron in octahedral sites, were also reported by Semenov (1969) and Chukanova et al. (2002). Type material of ferrisepiolite is deposited in the collections of the Geological Museum of China with catalogue number M11786.

2. Geographic location and geological occurrence

The Saishitang copper deposit is located on the Tibet-Qinghai Plateau at $99°47'15''E$, $35°17'15''N$ with an altitude of 3600–4000 m, about 230 km southwest of Xining, the capital city of Qinghai Province. The deposit was formed as a result of the interaction of Indo-Sinian granitic intrusions with Permian metamorphosed clastic and carbonate rocks. The copper orebodies, with total copper metal reserve of about 374,000 tons (on-site mine data), are closely associated with layered skarn distributed along the Lower Permian strata (Fig. 1). The deposit is currently mined by West Mining Co. of China on three levels at 3350 m, 3400 m and 3450 m.

Ferrisepiolite is easily observed in copper orebodies on all three production levels and in drill cores. It occurs as veinlets, 2 mm to 1 cm in thickness, crosscutting and replacing chalcopyrite, pyrrhotite, pyrite, sphalerite and galena hosted by hedenbergite–andradite–actinolite–vesuvianite skarn. Rounded grains of calcite and siderite are also present as inclusions in ferrisepiolite. In contrast, ferrisepiolite is not observed in Permian strata and in neighbouring quartz diorite. According to the mine geologists, the recovery of copper in the processing mill is sometimes decreased by high abundance of ferrisepiolite in the ores. The paragenetic relationships of ferrisepiolite with other minerals show that the late-stage ferrisepiolite was formed in a highly oxidizing environment from low-temperature Fe-rich fluids and crystallized in cavities and fractures within the skarn-ore deposit.
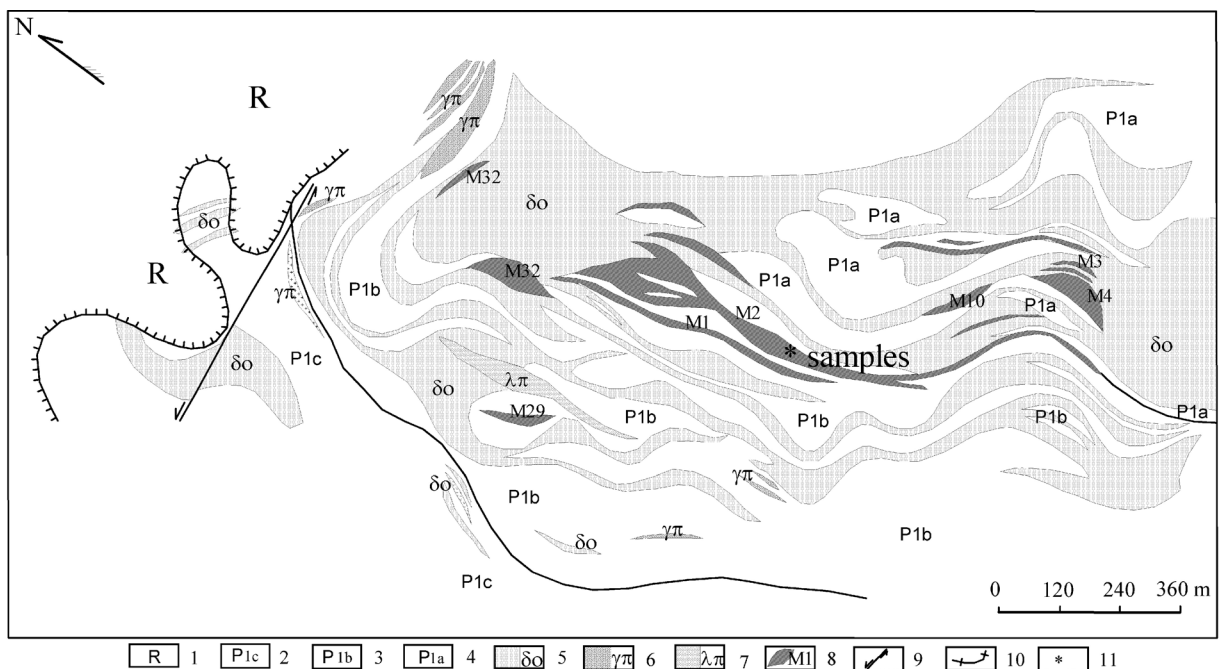

Fig. 1. Geological map on the 3400 m level in the Saishitang copper deposit (map supplied by the Mine). 1. Tertiary red sandstone with interbeds of clay mud; 2. Lower Permian banded marble and sericitic phyllite. 3. Lower Permian banded marble and biotitic phyllite; 4. Lower Permian meta-siltstone and biotitic phyllite; 5. Quartz diorite; 6. Granite porphyry; 7. Quartz porphyry. 8. Orebody number; 9. Faults; 10. Unconformity boundary; 11. Sampling locations.

3. Physical and optical properties

Ferrisepiolite occurs in two forms of aggregates: (a) as a brown earthy mass consisting of individual grains of flaky-acicular microlites with poor crystallinity, a few micrometres or less in size(Fig. 2a, b) as a brown fibrous aggregate with an appearance of wood bark, consisting of fibrous crystals several micrometres in width and more than several centimeters in length with good crystallinity (Fig. 2b). Both forms of ferrisepiolite are not magnetic based on a hand magnet test and they do not dissolve in dilute hydrochloric acid. Crystals are low in hardness at 2–2.5 and they have a brown streak. The crystallinity of ferrisepiolite is apparently related to the chemical composition. Poorly-crystallized earthy ferrisepiolite has high Fe_2O_3 + FeO contents (42.64%) and low MgO contents (1.78%), whereas well-crystallized fibrous ferrisepiolite is lower in Fe_2O_3 + FeO (average 27.30%) and higher in MgO (8.61%) (Table 1).

In reflected light, brown earthy ferrisepiolite in polished section is featured by low reflectance, weak anisotropism, and networked microfissures (Fig. 3a, b), whereas fibrous ferrisepiolite shows clear bireflectance and strong anisotropism. In polarized transmitted light, brown earthy ferrisepiolite in thin section shows brown colour with weak pleochroism with 1st order yellow to red interference colour (Fig. 3c, d), whereas fibrous ferrisepiolite is distinctly pleochroic from light red brown (for light vibrating perpendicular to the fibre axis) to dark red brown (for light vibrating parallel to the fibre axis). Although masked by the strong absorption colour, its birefringence is appreciable and exhibits up to 2nd order interference colours in thin sections of ~30 µm thickness (Fig. 3e, f). Attempts to measure refractive indices from brown earthy ferrisepiolite were difficult because of poor crystallinity and insufficient size. Small chips of fibrous ferrisepiolite were extracted for measurements of refractive indices in white light by the oil immersion method with the results: $\gamma' = 1.628(8)$, $\alpha' = 1.592–1.620$, $\gamma||c$, α (or β)$||a$, which are appreciably higher than those of sepiolite (1.515–1.529) (see http://www.handbookofmineralogy.org/pdfs/sepiolite.pdf) and Fe- and Mn-bearing sepiolite (1.557–1.597) (Chukanova *et al.* 2002).

The compatibility index (CI) calculated from measured refractive indices and the chemical composition of fibrous ferrisepiolite is equal to 0.02, which is considered an "excellent" value showing the consistency of the variation of refractive indices with chemical compositions (Mandarino, 1976, 1979, 1981).

4. Thermal analysis

The differential thermal analysis (DTA) and thermogravimetric (TG) data of ferrisepiolite were obtained from a Netzsch STA 490PC thermoanalyzer in the temperature range of 30–1000 °C at 10 K/min in an open container with nitrogen atmosphere. Three endothermic stages are shown in the DTA curve of ferrisepiolite (Fig. 4). The range 30–200 °C (peak at 102–130 °C) represents the loss of hygroscopic and zeolitic water accounting for about 12.30–15.7% of the total weight, the shoulder in the range 200–500 °C (centre at 273–290 °C) represents the loss of bound H_2O for about 4.59–4.95% of the total weight and the range 500–700 °C (peak at 607 °C) represents loss of bound hydroxyl for 0.1–0.9% of the total weight. The exothermic valley at 745–755 °C represents the decomposition of ferrisepiolite into magnetite, hematite, quartz and/or pigeonite as confirmed by XRD analysis of the product. The sharp valley at 93–115 °C in the differential TG curve may indicate the change from losing hygroscopic water to zeolitic water. The subtraction of H_2O contents in chemical analyses (Table 1) from the total mass losses in TG analyses, 20.70 wt% and 18.20 wt%, yields the mass loss of hygroscopic water, 6.30 wt% and 2.96 wt% respectively for earthy and fibrous ferrisepiolite. The higher hygroscopic water contents in earthy ferrisepiolite (6.30 wt%) than fibrous ferrisepiolite (2.96 wt%) is attributed to the formation of internal networked microfissures as shown in Fig. 3a, b.

Two or more stages of dehydration of bound water in the range of 200–500 °C, reported in sepiolite (Preisinger, 1959; Nagata *et al.* 1974, Yang & Zhang, 1994; Frost *et al.* 2009), are not observed in ferrisepiolite. The dehydration temperature of structural hydroxyl below 700 °C for ferrisepiolite is apparently lower than that of sepiolite (around 810–830 °C, *e.g.*, Frost *et al.* 2009), which may
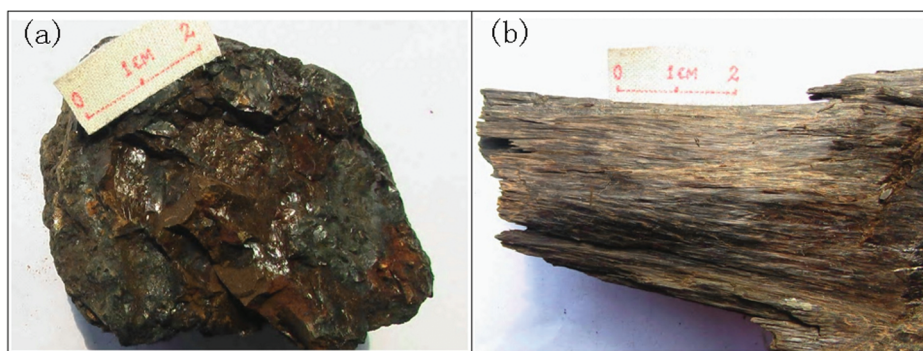

Fig. 2. Macroscopic forms of ferrisepiolite aggregates: (a) brown earthy aggregate, poorly crystallized, (b) brown fibrous aggregate, well crystallized.

Table 1. Chemical composition of ferrisepiolite.

Sample forms	Anal. No.	Weight percent (%)										Method
		SiO_2	Fe_2O_3[a]	FeO[a]	MgO	MnO	CaO	Na_2O	H_2O_{calc}	H_2O_{meas}	Total	
Brown earthy	ZD123_WET	38.89	34.97	7.28	2.05	0.48	0.71	0.15	14.19	14.73	98.72	Wet
	ZD123_XRF	40.76	34.59	7.20	1.80	0.46	0.75	0.14	13.96		99.67	XRF
	ZD123_EP01	40.78	34.76	7.24	1.81	0.48	0.85	0.27	14.09		100.28	EPMA
	ZD123_EP02	38.65	36.82	7.67	1.46	0.49	0.78	0.24	14.17		100.28	EPMA
	average	39.77	35.29	7.35	1.78	0.48	0.77	0.20	14.10	14.73	99.74	
Brown fibrous	ZD2151_WET	45.68	24.22	5.38	7.86	0.26	0.40	0.14	15.32	15.47	99.26	Wet
	ZD2151_XRF	47.17	23.94	5.38	7.55	0.23	0.46	0.12	15.09		99.95	XRF
	ZD2151_EP01	49.12	19.94	4.48	9.77	0.23	0.32	0.08	15.53		99.47	EPMA
	ZD2151_EP02	48.10	21.10	4.75	9.26	0.22	0.34	0.03	15.43		99.23	EPMA
	average	47.52	22.30	5.00	8.61	0.24	0.38	0.09	15.34	15.47	99.48	

Anal. No.	Atomic content per formula on the basis of 10 cations											
	Si	Fe^{3+}	Fe^{2+}	Mg	Mn	Ca	Na	O	ΣH_2O	OH	$Fe^{3+}{}_T$[b]	Molecular weight
ZD123_WET	5.13	3.47	0.80	0.40	0.05	0.10	0.04	16.85	6.15	0.31	0.87	780.79
ZD123_XRF	5.30	3.38	0.78	0.35	0.05	0.10	0.03	16.97	6.03	0.06	0.70	777.69
ZD123_EP01	5.26	3.37	0.78	0.35	0.05	0.12	0.07	16.91	6.09	0.17	0.74	777.56
ZD123_EP02	5.04	3.61	0.84	0.28	0.05	0.11	0.06	16.82	6.18	0.36	0.96	786.19
Average	5.18	3.46	0.80	0.35	0.05	0.11	0.05	16.89	6.11	0.23	0.82	780.56
ZD2151_WET	5.64	2.25	0.56	1.45	0.03	0.05	0.03	16.74	6.26	0.51	0.36	734.98
ZD2151_XRF	5.76	2.20	0.55	1.37	0.02	0.06	0.03	16.85	6.15	0.30	0.24	733.58
ZD2151_EP01	5.91	1.80	0.45	1.75	0.02	0.04	0.02	16.80	6.20	0.40	0.09	718.31
ZD2151_EP02	5.84	1.93	0.48	1.68	0.02	0.04	0.01	16.80	6.20	0.40	0.16	722.95
Average	5.79	2.05	0.51	1.56	0.02	0.05	0.02	16.80	6.20	0.40	0.21	727.46

[a]The partition of ferrous and ferric iron in XRF and EPMA analyses is calculated according to weight ratio of Fe^{3+}/Fe^{2+} determined in wet analyses.
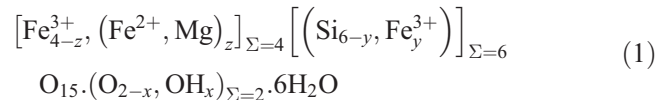[b]Fe^{3+} in tetrahedral site.

indicate that the bonding strength of hydroxyl is lower in ferrisepiolite. The mass loss of earthy ferrisepiolite in the range 500–700 °C is only ∼0.1%, although a clear endothermic effect occurs in the DTA curve, suggesting the deficiency of hydroxyl in the crystal structure.
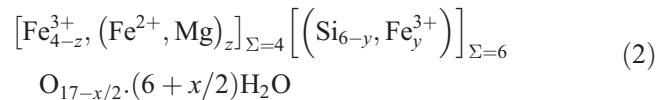
5. Chemical composition

The chemical composition of ferrisepiolite was determined separately by wet analysis, wavelength-dispersive X-ray fluorescence spectrometer (XRF) and electron probe microanalyzer (EPMA) methods (Table 1). Wet analyses were performed at the Changsha Research Institute of Mines and Metallurgy according to China National Standard Methods for bulk silicate analysis (GB/T 14506.1∼30-2010). XRF analysis was performed on pressed powder plate with a Rigaku Primus II spectrometer at 50 kV and 60 mA by means of the fundamental parameters (FP) method included in Rigaku software SQX. The EPMA analyses were performed with a JEOL JXA-8100 at 15 kV and 20 nA with the routine JEOL program. The back-scattered electron (BSE) image was used to determine the homogeneity of the composition (Fig. 3b). The partitioning of ferrous and ferric iron in XRF and EPMA analyses was calculated according to the weight ratio of

Fe^{3+}/Fe^{2+} (respectively equal to 4.32 and 4.05 for earthy and fibrous ferrisepiolite) as determined in wet analyses.

The calculated contents of H_2O in Table 1 are based on the assumption for the general formula of ferrisepiolite as:

$$\left[Fe^{3+}_{4-z}, \left(Fe^{2+}, Mg\right)_z\right]_{\Sigma=4} \left[\left(Si_{6-y}, Fe^{3+}_y\right)\right]_{\Sigma=6} \\ O_{15} \cdot (O_{2-x}, OH_x)_{\Sigma=2} \cdot 6H_2O \quad (1)$$

or equivalently,

$$\left[Fe^{3+}_{4-z}, \left(Fe^{2+}, Mg\right)_z\right]_{\Sigma=4} \left[\left(Si_{6-y}, Fe^{3+}_y\right)\right]_{\Sigma=6} \\ O_{17-x/2} \cdot (6 + x/2)H_2O \quad (2)$$

where y and z are determined from the metal oxide contents in the analyses by setting the total cation number equal to 10. The x value is determined as $x = 2*(17-O)$ from the total oxygen atom number $O = (17 - x/2)$ according to formula (2). The molecular number of H_2O is obtained from x value as $6 + x/2$ and the weight percent of H_2O is obtained by recalculating formula (2) with the result of 13.96–15.53% (Table 1). The results are in good agreement with the values of H_2O obtained by wet analyses and also similar to the weight loss of ferrisepiolite in the range of 80–700 °C of the thermal gravimetric data of ferrisepiolite.
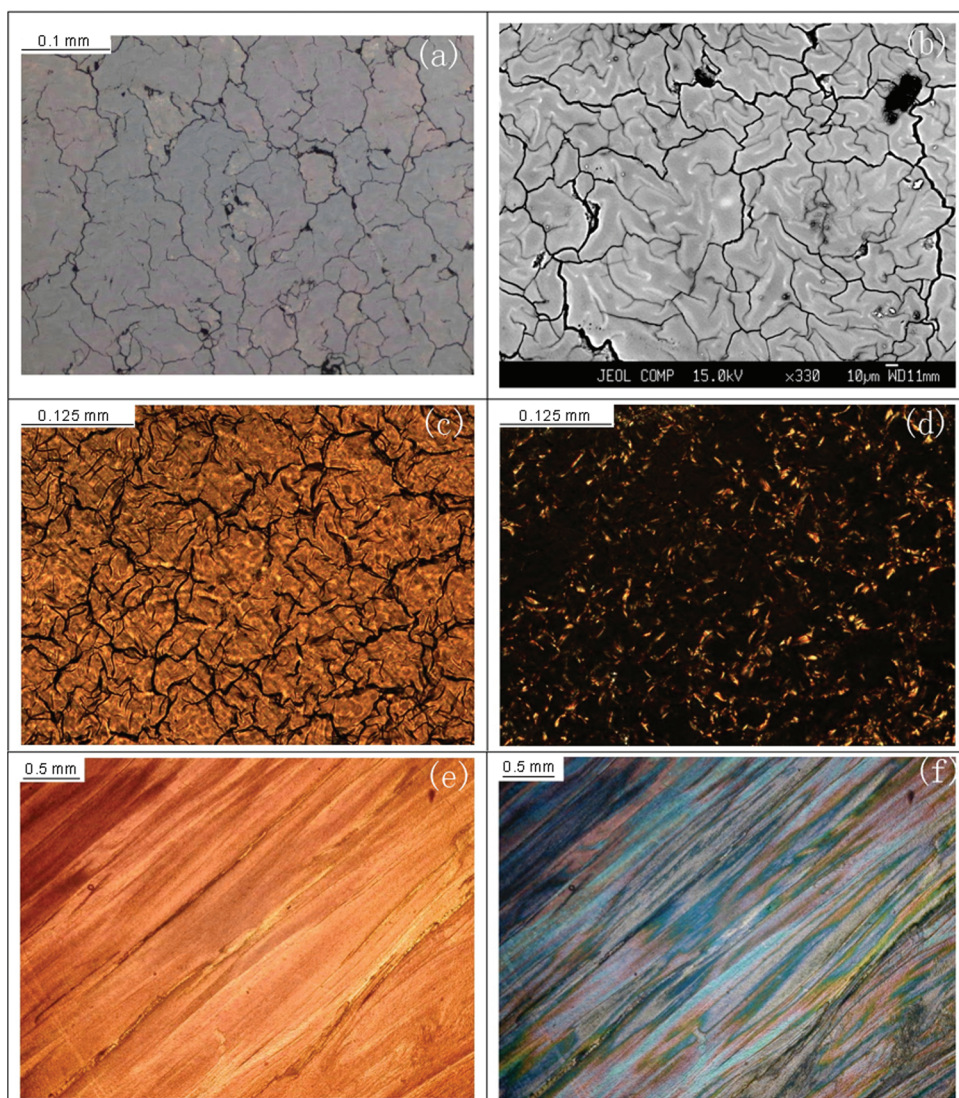
Fig. 3. Photomicrographs and BSE images of ferrisepiolite (a) Photomicrograph of brown earthy ferrisepiolite in reflected light with weak bireflectance and networked microfissures. (b) Backscattered-electron image of brown earthy ferrisepiolite, showing homogenous composition with networked microfissures. (c) Photomicrograph of brown earthy ferrisepiolite in thin section in parallel nicols, showing brown flaky-acicular microlites with weak pleochroism. (d) Photomicrograph of brown earthy ferrisepiolite in crossed nicols, showing flaky-acicular microlites with 1st order yellow to red interference colours in a poorly crystallized (dark) groundmass. (e) Photomicrograph of fibrous ferrisepiolite in thin section cut along the length of the fibre in parallel nicols, showing red brown colour with pleochroism from dark brown along the fibre length to light red perpendicular to the fibre length. (f) Photomicrograph of fibrous ferrisepiolite in thin section cut along the fibre length in crossed nicols, showing fibrous crystals with interference colour from 1st order yellow to 2nd order green.

The average chemical compositions of earthy and fibrous ferrisepiolite are, respectively, $(Fe^{3+}_{2.64}, Fe^{2+}_{0.80}, Mg_{0.35}, Ca_{0.11}, Mn_{0.05}, Na_{0.05})_{\Sigma=4}(Si_{5.18}, Fe^{3+}_{0.82})_{\Sigma=6}O_{15}.(O_{1.77}, OH_{0.23})_{\Sigma=2} \cdot 6H_2O$ and $(Fe^{3+}_{1.84}, Fe^{2+}_{0.51}, Mg_{1.56}, Ca_{0.05}, Mn_{0.02}, Na_{0.02})_{\Sigma=4}(Si_{5.79}, Fe^{3+}_{0.21})_{\Sigma=6}O_{15}.(O_{1.60}, OH_{0.40})_{\Sigma=2} \cdot 6H_2O$. The substitution of Fe^{3+} and Fe^{2+} for Mg in sepiolite $Mg_4Si_6O_{15}(OH)_2 \cdot 6H_2O$ is compensated by substitution of Si^{4+} by Fe^{3+} and, mostly, of OH^- by O^{2-}. The general formula may be written as $(Fe^{3+}, Fe^{2+}, Mg)_4(Si, Fe^{3+})_6O_{15}.(O, OH)_2 \cdot 6H_2O$, which involves Fe^{3+} predominating over Fe^{2+} or Mg^{2+} in the octahedral sites and O^{2-} predominating over OH^- in the hydroxyl site with OH as low as 0.23.

There is also appreciable Fe^{3+}, as much as 0.21–0.82, substituting for Si^{4+} in the tetrahedral sites. The atom numbers of Fe^{3+} in octahedral sites, i.e. 2.60–2.68 for earthy ferrisepiolite and 1.71–1.96 for fibrous ferrisepiolite, and Fe^{3+} in tetrahedral sites, i.e. 0.70–0.96 for earthy ferrisepiolite and 0.09–0.36 for fibrous ferrisepiolite, are apparently greater than those of sepiolite in the literature, in which the atom numbers of Fe^{3+} in octahedral and tetrahedral sites were respectively less than 1.20 and 0.52 (Brauner & Preisinger, 1956; Strunz, 1957; Preisinger, 1959; Binzer & Karup-Møller, 1974; García-Romero & Suárez, 2010). Moreover, the composition of earthy
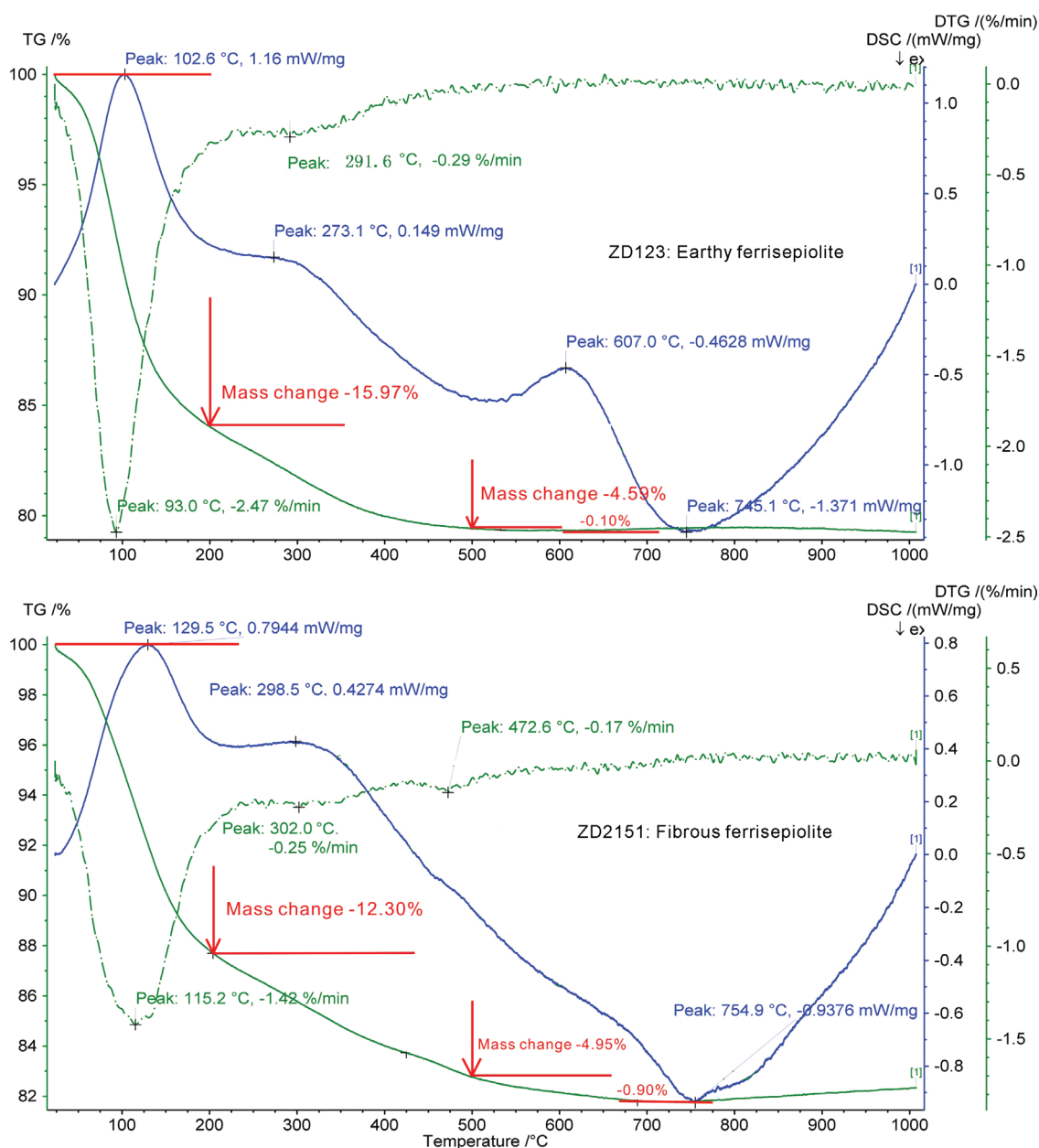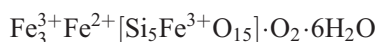
Fig. 4. Thermal analyses of earthy and fibrous ferrisepiolite: blue solid line-DTA curve, green solid line-TG curve, green dash line-differential TG curve.

ferrisepiolite may suggest the possibility of a dehydroxylated Fe(III) end-member of sepiolite with the formula of

$$Fe_3^{3+}Fe^{2+}[Si_5Fe^{3+}O_{15}] \cdot O_2 \cdot 6H_2O$$

Based on the chemical compositions of ferrisepiolite given in Table 1, the content (weight percent) of zeolitic water, bound H_2O, and structural hydroxyl (released in the form of H_2O) are 14.33%, 9.22% and 0.28% for earthy ferrisepiolite, 9.90%, 4.95% and 0.49% for fibrous ferriseiolite. These results are comparable to the mass loss of ferrisepiolite in the temperature ranges of 80–200 °C, 200–500 °C, and 500–700 °C as shown in Fig. 4.

6. Powder X-ray diffraction and crystallographic data

Powder samples of earthy and fibrous ferrisepiolite were measured for X-ray diffraction on a Rigaku D/Max 2500 diffractometer at 40 kV and 250 mA (Cu$K\alpha$) with a scanning speed 0.02 °/s. Oriented polished sections of fibrous ferrisepiolite, respectively parallel and perpendicular to the fibre direction, were measured on Rigaku D/Max Rapid IIR microdiffractometer at 40 kV and 250 mA (Cu$K\alpha$) with the collimator of 0.05 mm and 1 h exposure. Silicon powder was also measured at the same conditions and the data were used for calibration. Samples of sepiolite of low iron
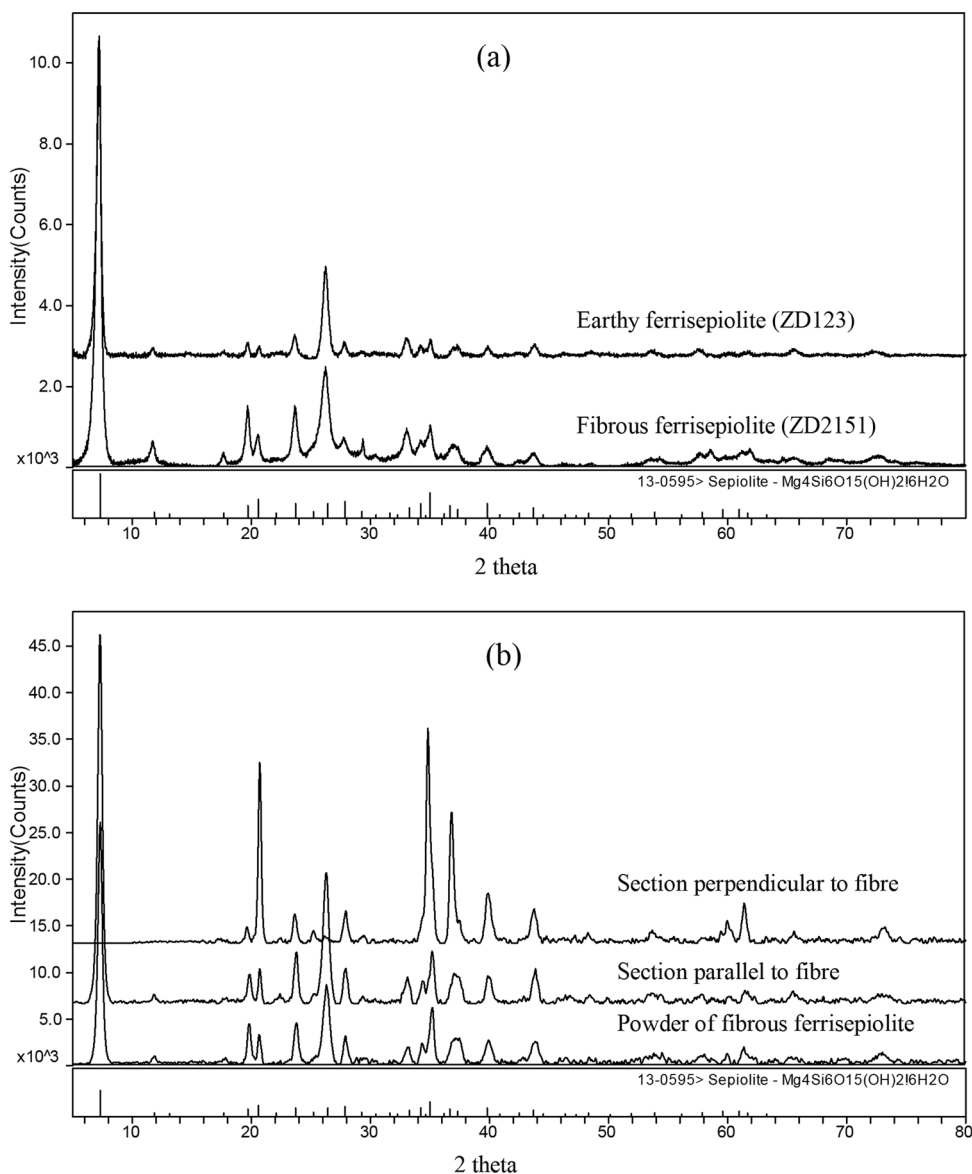
Fig. 5. X-ray diffraction patterns of ferrisepiolite (peak data listed in Table 2) with ICDD reference (No. 13-595). (a) Powder XRD patterns measured on Rigaku D/max 2500 diffractometer. (b) XRD patterns measured on Rigaku D/max Rapid IIR diffractometer, note that the peaks absent from the pattern obtained from the section perpendicular to the fibre axis are $(hk0)$ reflections.

contents (total iron $<$ 1 wt%) from Ningxiang and Xiangtan of Hunan Province were also measured for comparison. Representative XRD patterns are shown in Fig. 5 and the peak data are given in Table 2. The patterns and peak data are in good agreement with those of sepiolite from ICDD pdf No. 13-0595 and 26-1226, suggesting ferrisepiolite is isostructural with sepiolite, probably with space group *Pncn* (Preisinger, 1959; Brindley, 1959; Nagata *et al*. 1974). The diffraction lines are indexed according to the calculated powder pattern from the crystal structure data of Brauner & Preisinger (1956) and Post *et al*. (2007). The $(hk0)$ and $(h00)$ reflections in polished sections parallel to the fibre are absent in polished sections perpendicular to the fibre, indicating that the elongation of

the fibre is [001] (the **c**-axis). Sixteen strong lines were selected for refinement of unit-cell parameters using the method and program of Holland & Redfern (1997), with the results $a = 13.638\ (9)$, $b = 27.011\ (30)$, $c = 5.233\ (8)$ Å, $V = 1927.58\ \text{Å}^3$, $Z = 4$ for earthy ferrisepiolite and $a = 13.619\ (8)$, $b = 26.959\ (26)$, $c = 5.241\ (7)$ Å, $V = 1924.08$ Å^3, $Z = 4$ for fibrous ferrisepiolite.

In comparison to the unit-cell data of sepiolite from Nagata *et al*. (1974); Post *et al*. (2007) and Sánchez del Río *et al*. (2011): $a = 13.224–13.618$ (average 13.372 Å), $b = 26.731–27.383$ (average 27.005 Å), $c = 5.266–5.281$ (average 5.276 Å), $V = 1890.17–1911.89$ (average 1905.06 Å^3), ferrisepiolite has a smaller c parameter but larger a parameter and cell volume V, indicating that the

Table 2. Powder X-ray diffraction and crystallographic data of ferrisepiolite.[a]

	Fibrous ferrisepiolite (ZD2151)				Earthy ferrisepiolite (ZD123)					
I%	d_{obs} (Å)	d_{cal} (Å)	$d_{obs} - d_{cal}$	I%	d_{obs} (Å)	d_{cal} (Å)	$d_{obs} - d_{cal}$	h	k	l
100.0	**12.163**	**12.156**	**0.007**	**100.0**	**12.182**	**12.174**	**0.008**	**1**	**1**	**0**
3.1	7.516	7.501	0.015	2.6	7.519	7.514	0.005	1	3	0
1.3	6.741	6.740	0.001					0	4	0
1.4	5.139	5.145	−0.005					0	1	1
2.1	5.005	5.013	−0.008	1.1	5.040	5.023	0.018	1	5	0
5.1	4.525	4.527	−0.002					0	3	1
11.3	**4.487**	**4.493**	**−0.007**	**4.7**	**4.495**	**4.502**	**−0.007**	**0**	**6**	**0**
34.9	**4.298**	**4.296**	**0.002**	**3.2**	**4.296**	**4.294**	**0.002**	**1**	**3**	**1**
1.9	3.973	3.969	0.003					2	2	1
14.7	**3.751**	**3.750**	**0.000**	**6.4**	**3.760**	**3.757**	**0.003**	**2**	**6**	**0**
2.0	3.530	3.536	−0.006					2	4	1
29.1	**3.394**	**3.405**	**−0.011**	**30.8**	**3.393**	**3.410**	**−0.016**	**4**	**0**	**0**
12.7	**3.198**	**3.206**	**−0.007**	**4.2**	**3.209**	**3.207**	**0.002**	**3**	**3**	**1**
2.3	3.045	3.050	−0.005	1.2	3.045	3.052	−0.007	2	6	1
2.0	2.943	2.937	0.006	1.1	2.945	2.942	0.003	3	7	0
2.1	2.816	2.824	−0.008					2	7	1
2.2	2.784	2.775	0.009					1	8	1
6.4	**2.704**	**2.710**	**−0.006**	**6.0**	**2.706**	**2.714**	**−0.008**	**5**	**1**	**0**
8.5	**2.613**	**2.617**	**−0.004**	**2.5**	**2.620**	**2.619**	**0.000**	**2**	**8**	**1**
45.1	**2.561**	**2.554**	**0.006**	**4.9**	**2.560**	**2.557**	**0.003**	**1**	**9**	**1**
30.7	**2.436**	**2.436**	**0.001**	**2.6**	**2.429**	**2.433**	**−0.004**	**2**	**1**	**2**
10.1	**2.405**	**2.404**	**0.000**	**2.7**	**2.406**	**2.407**	**−0.001**	**3**	**8**	**1**
13.6	**2.260**	**2.257**	**0.004**	**3.7**	**2.260**	**2.259**	**0.001**	**3**	**9**	**1**
1.5	2.122	2.120	0.003	0.9	2.130	2.123	0.007	3	10	1
10.5	**2.068**	**2.067**	**0.002**	**3.9**	**2.064**	**2.069**	**−0.005**	**4**	**9**	**1**
2.0	1.961	1.964	−0.003	1.4	1.961	1.966	−0.005	5	8	1
2.5	1.882	1.885	−0.003	1.0	1.884	1.885	−0.001	4	6	2
4.0	**1.710**	**1.716**	**−0.006**					**6**	**0**	**2**
2.6	1.691	1.692	−0.001					1	12	2
1.7	1.649	1.648	0.000					6	10	1
2.9	1.593	1.597	−0.003	2.0	1.602	1.598	0.004	3	12	2
1.3	1.568	1.575	−0.007					1	17	0
4.8	**1.542**	**1.541**	**0.001**	**1.4**	**1.538**	**1.540**	**−0.002**	**1**	**8**	**3**
7.4	**1.509**	**1.509**	**0.000**	**1.1**	**1.510**	**1.508**	**0.001**	**0**	**9**	**3**
1.5	1.468	1.475	−0.008					7	6	2
3.8	1.424	1.424	0.000	2.2	1.421	1.426	−0.005	8	9	1
1.5	1.346	1.348	−0.001	0.7	1.355	1.347	0.007	5	8	3
4.1	1.294	1.294	0.000	1.3	1.303	1.296	0.007	1	18	2
3.7	1.274	1.277	−0.003					2	18	2

$a = 13.619\,(8)$, $b = 26.959\,(26)$, $c = 5.241\,(7)$ Å
$V = 1924.08$ Å^3, $Z = 4$, $d_{cal} = 2.51$ g/cm^3

$a = 13.638\,(9)$, $b = 27.011\,(30)$, $c = 5.233\,(8)$ Å
$V = 1927.58$ Å^3, $Z = 4$, $d_{cal} = 2.69$ g/cm^3

[a]Bold lines are used for unit-cell refinement with the method of Holland & Redfern (1997)

coupled substitution of Fe^{3+} and/or Fe^{2+} for Mg^{2+}; Fe^{3+} for Si^{4+}; and O^{2-} for OH^- may be accompanied by unit-cell contraction along the **c**-axis and expansion along the **a**-axis with an increase of the cell volume. It is also noted that the (040) reflection at 6.7 Å, commonly seen in sepiolite, is not observed in ferrisepiolite, which may be related to the substitution of Fe^{3+} and Fe^{2+} for Mg^{2+} and Si^{4+}, as also shown by Binzer & Karup-Møller (1974).

The powder XRD data of ferrisepiolite are also comparable to those of falcondoite $(Ni,Mg)_4Si_6O_{15}(OH)_2 \cdot 6H_2O$ and loughlinite $Na_2Mg_3Si_6O_{16} \cdot 8H_2O$ (Springer, 1976; Fahey *et al*. 1960). These minerals are classified into the palygorskite–sepiolite group of modulated-layer phyllosilicate with joined strips.

7. TEM and electron diffraction

Powder samples of earthy and fibrous ferrisepiolite were placed in glass vials with 10 ml ethanol and sonicated in a bath for 10 min to produce a powder suspension. Drops of the suspensions were deposited on copper grids (300 mesh) coated with carbon film. The dried copper grids were observed on a Fei Tecnai G2-ST electron transmission microscope at 200 kV and well-shaped crystals were selected for electron diffraction as shown in Fig. 6.

The TEM images show that earthy ferrisepiolite consists principally of poorly crystallized, irregularly rounded grains mixed with acicular crystals of 20–30 nm width. Fibrous ferrisepiolite is mainly composed of fragmented
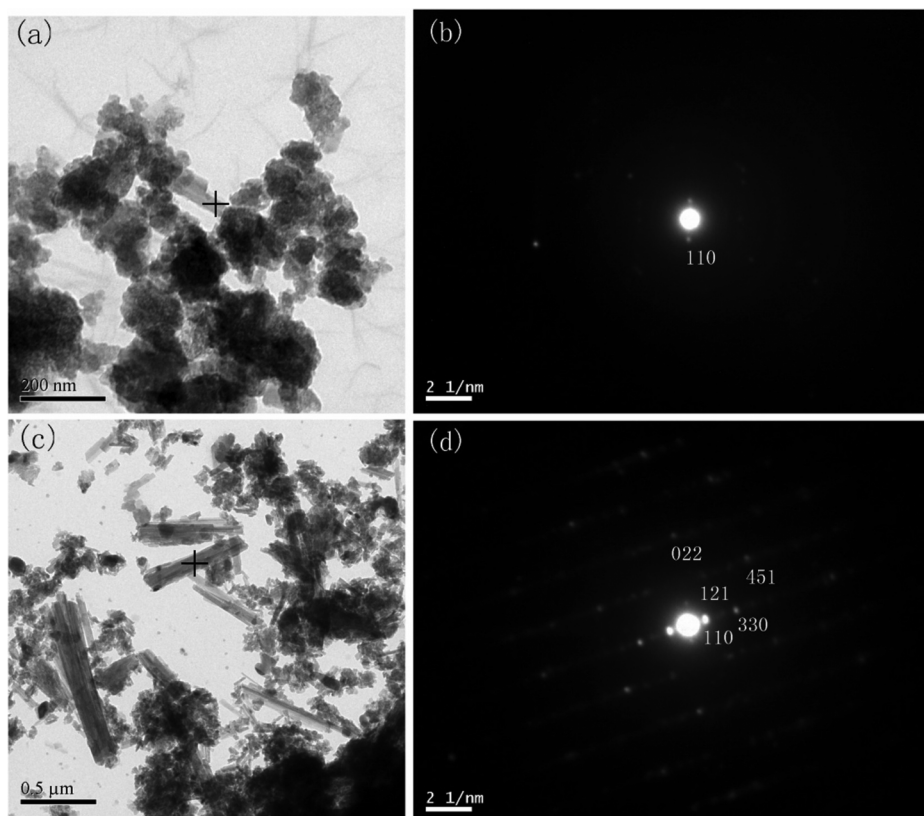
Fig. 6. TEM images and electron diffraction pattern of ferrisepiolite (a) Earthy ferrisepiolite sample: composed of poorly crystallized, irregularly rounded grains with acicular crystals. (b) Earthy ferrisepiolite sample: electron diffraction pattern of an euhedral crystal with the characteristic 110 reflection, the zone axis is not defined. (c) Fibrous ferrisepiolite sample: composed of fragmented fibrous crystals and irregular grains. (d) Fibrous ferrisepiolite sample: electron diffraction pattern on a fibrous crystal along $[1\bar{1}1]$ zone axis, indices of the reflections satisfying $k = h + l$ in accord with the lattice for sepiolite.

fibrous crystals and irregular grains 10–50 nm in width. The electron diffraction patterns of euhedral crystals in both samples feature the 110 refection, in addition to other reflections of the lattice as displayed by Brindley (1959) and Sánchez del Río *et al*. (2011).

References

Binzer, K. & Karup-Møller, S. (1974): Ferrisepiolite in hydrothermal calcite quartz chalcedony veins on Nuggsuag in West Greenland. *Bull. Grønlands Geol. Unders.*, **114**, 1–16.

Brauner, K. & Preisinger, A. (1956): Struktur und Entstehung des Sepioliths. *Tschermaks Min. Petr. Mitt.*, **5**, 120–140.

Brindley, G.W. (1959): X-ray and electron diffraction data for sepiolite. *Am. Mineral.*, **44**, 495–500.

Bøggild, O.B. (1951): Gunnbjarnite, a new mineral from East Greenland. *Medd. Gronland.*, **142**, 1–11.

Caillère, S. (1936): Contribution à l'étude des minéraux des serpentines. *Bull. Soc. Fr. Minéral.*, **59**, 163–326.

Chukanova, V.W., Pekov, I.V., Chukanov, N.V., Zadov, A.E. (2002): Iron-rich analogue of sepiolite and the conditions of its formation in the contact aureole of the Lovozero alkaline massif. *Geochem. Int*., **40**, 1225–1229.

Fahey, J.J., Ross, M., Axelrod, J.M. (1960): Loughlinite, a new hydrous sodium magnesium silicate. *Am. Mineral.*, **45**, 270–281.

Frost, R.L., Kristóf, J., Horváth, E. (2009): Controlled rate thermal analysis of sepiolite. *J. Therm. Anal. Calorim.*, **98**, 749–755.

García-Romero, E. & Suárez, M. (2010): On the chemical composition of sepiolite and palygorskite. *Clays Clay Minerals*, **58**, 1–20.

Holland, T.J.B. & Redfern, S.A.T. (1997): Unit cell refinement from powder diffraction data: the use of regression diagnostics. *Mineral. Mag.*, **61**, 65–77.

Mandarino, J.A. (1976): The Gladstone-Dale relationship-Part I: Derivation of new constants. *Can. Mineral.*, **14**, 498–502.

— (1979): The Gladstone-Dale relationship-Part III: Some general applications. *Can. Mineral.*, **17**, 71–76.

— (1981): The Gladstone-Dale relationship: Part IV: The compatibility concept and its application. *Can. Mineral.*, **19**, 441–450.

Nagata, H., Shimoda, S., Sudo, T. (1974): On dehydration of bound water of sepiolite. *Clays Clay Minerals*, **22**, 285–293.

Post, J.E., Bish, D.L., Heaney, P.J. (2007): Synchrotron powder X-ray diffraction study of the structure and dehydration behavior of sepiolite. *Am. Mineral.*, **92**, 91–97.

Preisinger, A. (1959): X-ray study of the structure of sepiolite. *Clays Clay Minerals*, **6**, 61–67.

Sánchez del Río, M., García-Romero, E., Suárez, M., Silva, I., Fuentes-Montero, L., Martínez-criado, G. (2011): Variability in sepiolite: diffraction studies. *Am. Mineral.*, **96**, 1443–1454.

Semenov, E.I. (1969): Mineralogy of the Ilimaussaq Alkaline Massif, Southern Greenland. *Inst. Mineral. Geokhim. Kristallokhim. Redk Elementov, Izdat. Nauka.*, **164**, 103–106 (in Russian, abstracted in *Am. Mineral.* **55**, 2138).

Smith, D.G.W. & Nickel, E.H. (2007): A system for codification for unnamed minerals: report of the Subcommittee for Unnamed Minerals of the IMA Commission on New Minerals, Nomenclature and Classification. *Can. Mineral.*, **45**, 983–1055.

Springer, G. (1976): Falcondoite, nickel analogue of sepiolite. *Can. Mineral.*, **14**, 407–409.

Strunz, H. (1957): Gunnbjarnit, ein Ferri-Sepiolith. *N. Jb. Miner. Mh.*, **1**, 75–77.

Yang, Y.X. & Zhang, N.X. (1994): Clay minerals in China. Geological Press, Beijing, 297 p.